PNAS RESEARCH ARTICLE | NEUROSCIENCE

The autism-associated loss of δ-catenin functions disrupts social behavior

Hadassah Mendez-Vazquez[a,1], Regan L. Roach[a,1], Kaila Nip[b,1,2], Soham Chanda[b,c,d], Matheus F. Sathler[a], Tyler Garver[c], Rosaline A. Danzman[a], Madeleine C. Moseley[c], Jessica P. Roberts[c], Olivia N. Koch[a], Ava A. Steger[e], Rahmi Lee[a], Jyothi Arikkath[f], and Seonil Kim[a,b,c,3]

Edited by Michael Greenberg, Harvard Medical School, Boston, MA; received January 14, 2023; accepted May 1, 2023

δ-catenin is expressed in excitatory synapses and functions as an anchor for the glutamatergic AMPA receptor (AMPAR) GluA2 subunit in the postsynaptic density. The glycine 34 to serine (G34S) mutation in the *δ-catenin* gene has been found in autism spectrum disorder (ASD) patients and results in loss of δ-catenin functions at excitatory synapses, which is presumed to underlie ASD pathogenesis in humans. However, how the G34S mutation causes loss of δ-catenin functions to induce ASD remains unclear. Here, using neuroblastoma cells, we identify that the G34S mutation increases glycogen synthase kinase 3β (GSK3β)-dependent δ-catenin degradation to reduce δ-catenin levels, which likely contributes to the loss of δ-catenin functions. Synaptic δ-catenin and GluA2 levels in the cortex are significantly decreased in mice harboring the δ-catenin G34S mutation. The G34S mutation increases glutamatergic activity in cortical excitatory neurons while it is decreased in inhibitory interneurons, indicating changes in cellular excitation and inhibition. δ-catenin G34S mutant mice also exhibit social dysfunction, a common feature of ASD. Most importantly, pharmacological inhibition of GSK3β activity reverses the G34S-induced loss of δ-catenin function effects in cells and mice. Finally, using δ-catenin knockout mice, we confirm that δ-catenin is required for GSK3β inhibition-induced restoration of normal social behavior in δ-catenin G34S mutant animals. Taken together, we reveal that the loss of δ-catenin functions arising from the ASD-associated G34S mutation induces social dysfunction via alterations in glutamatergic activity and that GSK3β inhibition can reverse δ-catenin G34S-induced synaptic and behavioral deficits.

autism | delta-catenin | social behavior | AMPA receptors

Social behavior is essential for the survival of many species (1). However, our knowledge of the physiological, cellular, and molecular mechanisms driving social behavior is still limited (1). Moreover, various mental disorders, including autism spectrum disorder (ASD), anxiety, depression, and schizophrenia, have social impairment as a primary symptom (2–5). Therefore, improved knowledge of the mechanisms mediating social behavior can help us to better understand these diseases and develop effective treatments.

A large body of studies illustrates the idea that varied synaptic activity and signaling contribute to the initiation, maintenance, and/or modulation of social behavior (1). However, the relationship between synaptic regulation and social behavior is not completely understood. Postsynaptic glutamatergic activity in excitatory and inhibitory cells in multiple brain regions is crucial for social behavior (6–10). In fact, disruptions in excitatory connectivity have been implicated in individuals with ASD and in mouse models of ASD (11–19). However, it is not well understood how postsynaptic glutamatergic activity regulates social behavior. Several human genetic studies suggest that the *δ-catenin* gene is strongly linked to ASD (20–24). Notably, genetic alterations in the *δ-catenin* gene are associated with severely affected ASD patients from multiple families (21, 23, 24). δ-catenin is a member of the armadillo repeat protein family that is highly expressed in neurons and localizes to the excitatory and inhibitory synapses (25–31). At the postsynaptic density (PSD) in the excitatory synapse, δ-catenin interacts with the intracellular domain of N-cadherin, a synaptic cell adhesion protein, and the carboxyl terminus of δ-catenin binds to AMPA-type glutamate receptor (AMPAR)-binding protein (ABP) and glutamate receptor-interacting protein (GRIP) (*SI Appendix*, Fig. S1) (25, 28–30, 32, 33). This N-cadherin-δ-catenin-ABP/GRIP complex functions as an anchor for the AMPAR GluA2 subunit (*SI Appendix*, Fig. S1) and is disrupted when δ-catenin functions are lost (25, 30, 34, 35). Importantly, some δ-catenin ASD mutations are unable to reverse the δ-catenin deficiency-induced loss of excitatory synapses in cultured mouse neurons, suggesting that these mutations cause a loss of δ-catenin functions (24). This indicates that δ-catenin deficiency induces ASD-associated social deficits via impairment of glutamatergic synapses. Moreover, δ-catenin expression is closely linked to other ASD-risk genes involved in synaptic structure and function, such as GluA2,

Significance

δ-catenin is important for the localization and function of glutamatergic AMPA receptors at synapses in many brain regions. The glycine 34 to serine (G34S) mutation in the *δ-catenin* gene has been found in autism patients and results in the loss of δ-catenin functions. δ-catenin expression is also closely linked to other autism-risk genes involved in synaptic structure and function, further implying that it is important for the development of autism. Importantly, social dysfunction is a key characteristic of autism. However, the links between δ-catenin functions and social behavior are largely unknown. The significance of the current research is thus predicated on filling this gap by identifying the molecular, cellular, and synaptic underpinnings of the role of δ-catenin in social behavior.

Author contributions: S.K. designed research; H.M.-V., R.L.R., K.N., S.C., M.F.S., T.G., R.A.D., M.C.M., J.P.R., O.N.K., A.A.S., and R.L. performed research; J.A. contributed new reagents/analytic tools; H.M.-V., R.L.R., K.N., S.C., M.F.S., R.A.D., M.C.M., and S.K. analyzed data; and H.M.-V, R.L.R., K.N., S.C., and S.K. wrote the paper.

The authors declare no competing interest.

This article is a PNAS Direct Submission.

[1]H.M.-V., R.L.R., and K.N. contributed equally to this work.

[2]Present address: Department of Cellular and Integrative Physiology, University of Texas Health Science Center San Antonio, San Antonio, TX 78229.

[3]To whom correspondence may be addressed. Email: seonil.kim@colostate.edu.

This article contains supporting information online at https://www.pnas.org/lookup/suppl/doi:10.1073/pnas.2300773120/-/DCSupplemental.

Published May 22, 2023.

cadherins, GRIP, and synaptic Ras GTPase activating protein 1 (SYNGAP1), further illustrating its importance for synaptic pathophysiology and social dysfunction in ASD (31, 36–38). Nonetheless, the molecular and cellular links between δ-catenin functions, synaptic activity, and social behavior are largely unknown.

Among the ASD-associated δ-catenin missense mutations, the glycine 34 to serine (G34S) mutation exhibits a profound loss of δ-catenin functions in excitatory synapses (24). However, how the δ-catenin G34S mutation causes the loss of δ-catenin functions to induce social deficits in ASD is not understood. Here, we reveal that the δ-catenin G34S mutation increases glycogen synthase kinase 3β (GSK3β)-mediated δ-catenin degradation. Using δ-catenin G34S knockin mice, we find that the δ-catenin G34S mutation significantly reduces synaptic δ-catenin and GluA2 levels in the cortex, markedly alters glutamatergic activity in cortical neurons, and impairs social behavior. Moreover, we show that a pharmacological reduction of GSK3β activity can reverse the G34S-induced loss of δ-catenin function effects on synaptic δ-catenin and GluA2 levels, glutamatergic activity, and social behavior. Finally, using δ-catenin knockout (KO) mice, we confirm that δ-catenin is required for GSK3β inhibition-induced restoration of normal social behavior in δ-catenin G34S animals. Importantly, recent studies suggest that changes in GSK3β activity may be an important aspect of the pathophysiology of ASD (39–46). Moreover, GSK3β is suggested to be a useful therapeutic target for brain disorders because GSK3β has been linked to cognitive processes (47). Therefore, our research not only identifies the molecular, cellular, and synaptic underpinnings of the role of δ-catenin in social behavior but also identifies GSK3β as a therapeutic target for limiting the loss of δ-catenin function-induced synaptic dysfunction in ASD and related mental disorders.

Results

The δ-Catenin G34S Mutation Increases GSK3β-Mediated δ-Catenin Degradation. It has been previously shown that GSK3β phosphorylates threonine 1078 (T1078) of δ-catenin, leading to δ-catenin ubiquitination and subsequent proteasome-mediated degradation, whereas inhibition of GSK3β elevates δ-catenin levels (29, 48, 49). GSK3β also phosphorylates β-catenin, another member of the armadillo-repeat proteins, and triggers its degradation in a similar manner (50, 51). In contrast to δ-catenin, which has a GSK3β-mediated phosphorylation site toward the carboxyl terminus (T1078), β-catenin has the phosphorylation sites at serine 33 and 37 (S33 and S37) and threonine 41 (T41) in the amino terminus (52) (*SI Appendix*, Fig. S2). The group-based prediction system (53) predicts that the G34S mutation in the amino terminus of δ-catenin mimics one of the β-catenin phosphorylation sites, which may increase the chances of GSK3β-mediated phosphorylation of δ-catenin (*SI Appendix*, Fig. S2). This likely accelerates the degradation of δ-catenin, causing the loss of δ-catenin functions. To address whether the δ-catenin G34S mutation increases GSK3β-mediated δ-catenin degradation, we expressed wild-type (WT) δ-catenin or G34S δ-catenin in human neuroblastoma (SH-SY5Y) cells that lack endogenous δ-catenin expression and compared δ-catenin levels using immunoblotting. When normalized to WT δ-catenin, G34S δ-catenin levels were significantly reduced (WT, 1.000 ± 0.286 and G34S, 0.592 ± 0.260, $P = 0.0227$) (*SI Appendix*, Fig. S3). To determine whether reduced G34S δ-catenin levels were mediated by proteasomal degradation, we treated cells with 10 μM MG132, a proteasome inhibitor, for 4 h and measured δ-catenin levels using immunoblotting. When proteasome activity was inhibited, both WT δ-catenin and mutant δ-catenin levels were significantly elevated in comparison to δ-catenin levels without MG132 treatment (WT + MG132, 2.659 ± 1.630, $P = 0.0066$, and G34S + MG132, 2.239 ± 1.658, $P = 0.0002$) (*SI Appendix*, Fig. S3). This suggests that the δ-catenin G34S mutation reduces δ-catenin levels, which is mediated by proteasomal degradation.

To examine whether reduced δ-catenin G34S expression was dependent on GSK3β, we used lithium chloride (LiCl) to inhibit GSK3β activity pharmacologically. We have previously shown that LiCl treatment significantly reduces GSK3β activity and increases δ-catenin levels in cultured mouse neurons and mouse brains (29). WT δ-catenin or G34S δ-catenin was expressed in SH-SY5Y cells, and these cells were treated with 2 mM LiCl or 2 mM sodium chloride (NaCl) for 18 h before collecting whole-cell lysates to analyze δ-catenin levels. We confirmed that mutant δ-catenin levels were significantly reduced in the absence of LiCl (WT + NaCl, 1.000 ± 0.287 and G34S + NaCl, 0.479 ± 0.208, $P = 0.0354$) (Fig. 1*A*). Importantly, LiCl treatment significantly elevated the levels of both WT δ-catenin and mutant δ-catenin (WT + LiCl, 1.456 ± 0.479, $P = 0.0300$, and G34S + LiCl, 1.336 ± 0.560, $P < 0.0001$) (Fig. 1*A*). We confirmed that LiCl treatment significantly reduced GSK3β activity in cells by showing that it markedly increased phosphorylation at serine 9 of GSK3β (pGSK3β), an inactive form of GSK3β (48, 49), as seen previously (29) (WT + NaCl, 1.000 ± 0.405 and WT + LiCl, 1.712 ± 0.644, $P = 0.0051$, and G34S + NaCl, 1.124 ± 0.433 and G34S + LiCl, 1.749 ± 0.635, $P = 0.0265$) (Fig. 1*A*). To account for potential offtarget effects from lithium treatment, we utilized siRNA for genetic inhibition of GSK3β. SH-SY5Y cells expressing WT δ-catenin or G34S δ-catenin were treated with either 25 nM scrambled siRNA as a control (CTRL) or 25 nM GSK3β siRNA for 72 h. When we compared the WT δ-catenin and G34S δ-catenin levels in cells treated with CTRL siRNA, a significantly reduced δ-catenin level was observed in cells expressing mutant δ-catenin (WT + CTRL siRNA, 1.000 ± 0.231 and G34S + CTRL siRNA, 0.478 ± 0.223, $P = 0.0429$) (Fig. 1*B*). Both WT δ-catenin and G34S δ-catenin levels were significantly elevated by GSK3β siRNA-mediated knockdown (WT + GSK3β siRNA, 1.485 ± 0.592, $P = 0.0365$, and G34S + GSK3β siRNA, 1.215 ± 0.596, $P = 0.0007$) (Fig. 1*B*). We confirmed that GSK3β siRNA significantly reduced GSK3β levels, indicating a decrease in GSK3β activity (WT + CTRL siRNA, 1.000 ± 0.196 and WT + GSK3β siRNA, 0.359 ± 0.208, $P < 0.0001$, and G34S + CTRL siRNA, 0.912 ± 0.442 and G34S + GSK3β siRNA, 0.481 ± 0.365, $P = 0.0017$) (Fig. 1*B*). Taken together, we identify that the δ-catenin G34S mutation increases GSK3β-mediated δ-catenin degradation to decrease δ-catenin levels via a proteasome-mediated mechanism, likely leading to loss of δ-catenin functions. We further reveal that the pharmacological or genetic reduction of GSK3β activity increases both WT and G34S δ-catenin levels.

Additional δ-Catenin Mutations Confirm Enhanced GSK3β-Dependent δ-Catenin Degradation in the G34S Mutation. Additional δ-catenin mutations were generated to test the hypothesis that the G34S mutation enhanced GSK3β-dependent δ-catenin degradation. First, we substituted the glycine 34 for alanine (A) to make a G34A mutant that would not be phosphorylated by GSK3β. We also generated a G34D mutant in which glycine was substituted with a phosphomimetic aspartate (D) at position 34. WT δ-catenin, G34A δ-catenin, or G34D δ-catenin was expressed in SH-SY5Y cells, and δ-catenin levels were measured using immunoblotting. We found that there was no significant difference between WT δ-catenin and G34A δ-catenin expression (WT, 1,000 and G34A, 1.311 ± 0.437, $P > 0.9999$) (Fig. 2*A*). However, G34D δ-catenin levels were significantly reduced, when

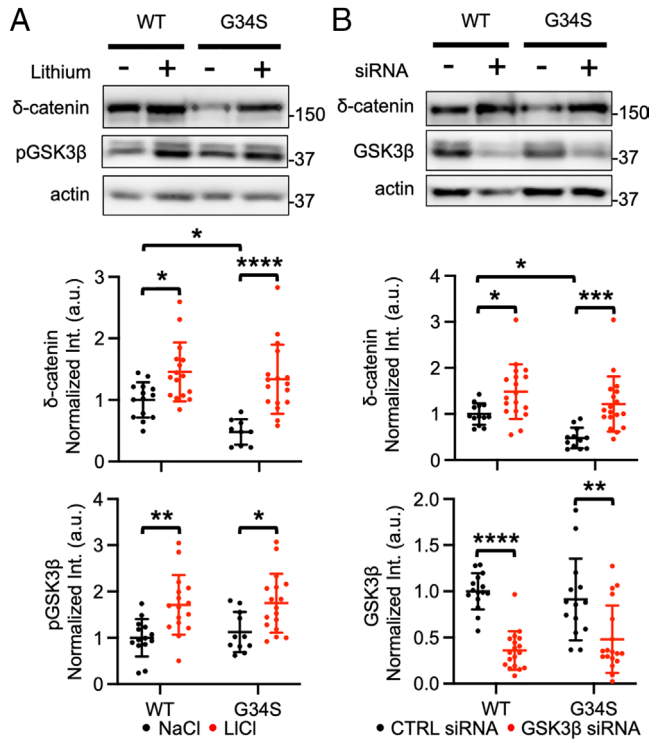

Fig. 1. The δ-catenin G34S mutation increases GSK3β-mediated δ-catenin degradation. (*A*) Representative immunoblots and summary graphs of normalized δ-catenin and pGSK3β levels in SH-SY5Y cell lysates transfected with WT or G34S δ-catenin and treated with 2 mM NaCl (−) or 2 mM LiCl (+) (n = number of immunoblots from five independent cultures. For δ-catenin, WT + NaCl = 14, WT + LiCl = 16, G34S + NaCl = 9, and G34S + LiCl = 17. For pGSK3β, WT + NaCl = 14, WT + LiCl = 16, G34S + NaCl = 11, and G34S + LiCl = 17. Two-way ANOVA with the Tukey test, **P* < 0.05, ***P* < 0.01, and *****P* < 0.0001). (*B*) Representative immunoblots and summary graphs of normalized δ-catenin and GSK3β levels in SH-SY5Y cell lysates transfected with WT or G34S δ-catenin and treated with scrambled (CTRL) (−) or GSK3β (+) siRNA (n = number of immunoblots from five independent cultures. For δ-catenin, WT + CTRL siRNA = 13, WT + GSK3β siRNA = 18, G34S + CTRL siRNA = 12, and G34S + GSK3β siRNA = 18. For GSK3β, WT + CTRL siRNA = 15, WT + GSK3β siRNA = 18, G34S + CTRL siRNA = 14, and G34S + GSK3β siRNA = 18. Two-way ANOVA with the Tukey test, **P* < 0.05, ***P* < 0.01, ****P* < 0.001, and *****P* < 0.0001). The position of molecular mass markers (kDa) is shown on the right of the blots. Mean ± SD.

compared with WT δ-catenin and G34A δ-catenin (G34D, 0.662 ± 0.150, WT vs. G34D, $P = 0.0088$, G34A vs. G34D, $P = 0.0088$) (Fig. 2*A*), as seen in cells expressing G34S δ-catenin (Fig. 1). Next, we used LiCl to pharmacologically inhibit GSK3β activity as shown in Fig. 1*A*. Given that G34A δ-catenin acted similarly to WT δ-catenin (Fig. 2*A*), G34A δ-catenin or G34D δ-catenin was expressed in SH-SY5Y cells, and cells were treated with 2 mM LiCl or 2 mM NaCl for 18 h. As seen in Fig. 2*A*, G34D δ-catenin levels were significantly reduced in the absence of LiCl when compared to G34A δ-catenin (G34A + NaCl, 1.000 ± 0.258 and G34D + NaCl, 0.551 ± 0.361, $P = 0.0101$) (Fig. 2*B*). LiCl treatment significantly elevated the levels of G34A δ-catenin, but not G34D δ-catenin (G34A + LiCl, 1.583 ± 0.458, $P = 0.0005$, and G34D + LiCl, 0.476 ± 0.255, $P = 0.9433$) (Fig. 2*B*). We confirmed that LiCl treatment significantly increased pGSK3β, an indication of GSK3β inhibition (G34A + NaCl, 1.000 ± 0.197 and G34A + LiCl, 1.601 ± 0.531, $P = 0.0317$, and G34D + NaCl, 0.982 ± 0.245 and G34D + LiCl, 1.557 ± 0.877, $P = 0.0372$) (Fig. 2*B*). Finally, we used GSK3β siRNA for genetic inhibition of GSK3β activity. G34A δ-catenin or G34D δ-catenin was expressed in SH-SY5Y cells with either 25 nM scrambled siRNA (CTRL) or 25 nM GSK3β siRNA for 72 h. When we compared the G34A δ-catenin and G34D δ-catenin levels in cells treated with scrambled siRNA, significantly reduced δ-catenin G34D levels were found (G34A + CTRL siRNA, 1.000 ± 0.166 and G34D + CTRL siRNA, 0.393 ± 0.230, $P = 0.0330$) (Fig. 2*C*). Like lithium treatment, GSK3β knockdown had no effect on G34D δ-catenin levels, but it significantly elevated G34A δ-catenin expression (G34A + GSK3β siRNA, 2.100 ± 0.841, $P < 0.0001$, and G34D + GSK3β siRNA, 0.594 ± 0.424, $P = 0.8190$) (Fig. 2*C*). As seen in Fig. 1*B*, GSK3β siRNA treatment significantly reduced GSK3β levels (G34A + CTRL siRNA, 1.000 ± 0.388 and G34A + GSK3β siRNA, 0.467 ± 0.137, $P = 0.0171$, and G34D + CTRL siRNA, 1.218 ± 0.599 and G34D + GSK3β siRNA, 0.479 ± 0.189, $P = 0.0013$) (Fig. 2*C*). This suggests the G34S mutation enhances GSK3β-mediated δ-catenin degradation, which likely contributes to loss of δ-catenin functions.

Lithium Treatment Reverses the Significant Reduction of Synaptic δ-Catenin and GluA2 in the δ-Catenin G34S Cortex. To understand how the G34S mutation affected δ-catenin and AMPAR levels in the brain, we used δ-catenin G34S knockin mice that were generated at University of Nebraska Medical Center (UNMC) Mouse Genome Engineering Core utilizing the CRISPR-Cas9 technique (54). The whole-tissue lysates and PSD fractions of the cortex were collected from 3-mo-old female and male WT and δ-catenin G34S animals and analyzed for total and synaptic protein levels, respectively, using immunoblotting. For whole-tissue lysates, we found no difference in total δ-catenin (WT female, 1.000 ± 0.406 and G34S female, 0.960 ± 0.294, $P = 0.8056$) and GluA2 (WT female, 1.000 ± 0.273 and G34S female, 0.843 ± 0.222, $P = 0.1748$) levels between the WT and G34S female cortex, while total δ-catenin (WT male, 1.000 ± 0.608 and G34S male, 0.318 ± 0.206, $P = 0.0035$) and GluA2 (WT male, 1.000 ± 0.571 and G34S male, 0.543 ± 0.280, $P = 0.0357$) levels were significantly lower in the male G34S cortex compared to the WT male cortex (*SI Appendix*, Fig. S4). However, there was no significant difference in total GluA1 (WT female, 1.000 ± 0.116 and G34S female, 0.991 ± 0.219, $P = 0.9335$, and WT male 1.000 ± 0.586 and G34S male, 0.835 ± 0.440, $P = 0.5930$) levels between the WT and G34S cortex (*SI Appendix*, Fig. S4). Notably, we found a significant reduction in synaptic δ-catenin (WT female, 1.000 and G34S female, 0.494 ± 0.334, $P = 0.0070$, WT male, 1.000 and G34S male, 0.494 ± 0.227, $P = 0.0348$) and GluA2 levels (WT female 1.000 and G34S female, 0.612 ± 0.192, $P = 0.0017$, WT male, 1.000 and G34S male, 0.540 ± 0.222, $P = 0.0440$) in the female and male G34S animals' cortices when compared to the WT cortex, but no difference in synaptic GluA1 levels (WT female 1.000 and G34S female, 0.943 ± 0.619, $P = 0.4723$, WT male, 1.000, and G34S male, 0.848 ± 0.206, $P = 0.3362$) between the WT and G34S cortex (Fig. 3 *A* and *B*). Next, synaptic δ-catenin and AMPAR levels in the hippocampus were similarly analyzed using immunoblotting. We found no difference in synaptic δ-catenin (WT female, 1.000 and G34S female, 0.929 ± 0.222, $P = 0.4344$, and WT male, 1.000 and G34S male, 0.847 ± 0.371, $P = 0.4843$), GluA1 (WT female, 1.000 and G34S female, 1.293 ± 0.457, $P = 0.3876$, and WT male, 1.000 and G34S male, 0.880 ± 0.311, $P = 0.8050$), and GluA2 levels (WT female, 1.000 and G34S female, 0.931 ± 0.366, $P = 0.3654$, and WT male, 1.000 and G34S male, 0.848 ± 0.206, $P = 0.9672$) between the WT and G34S hippocampus (*SI Appendix*, Fig. S5*A*). This suggests that the δ-catenin G34S mutation significantly reduces synaptic δ-catenin and GluA2 levels selectively in the cortex, but not in the hippocampus. This difference is likely due to higher GluA2 levels in the mouse hippocampus than the cortex (55, 56), thus GluA2 levels in the hippocampus are less affected by the δ-catenin G34S mutation compared to cortical GluA2 levels.

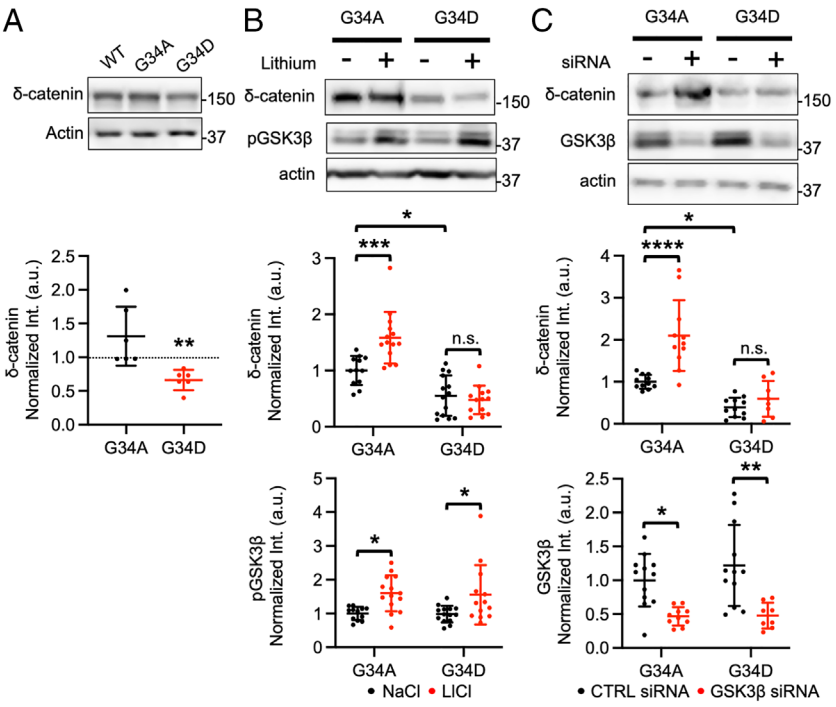

Fig. 2. Additional δ-catenin mutations confirm enhanced GSK3β-dependent δ-catenin degradation in the G34S mutation. (*A*) Representative immunoblots and summary graphs of normalized δ-catenin levels in SH-SY5Y cell lysates transfected with WT, G34A, or G34D δ-catenin (n = 6 immunoblots from three independent cultures, Kruskal–Wallis test with Dunn's test, $^{**}P < 0.01$). (*B*) Representative immunoblots and summary graphs of normalized δ-catenin and pGSK3β levels in SH-SY5Y cell lysates transfected with G34A or G34D δ-catenin and treated with 2 mM NaCl (−) or 2 mM LiCl (+) (n = number of immunoblots from three independent cultures. G34A + NaCl = 12, G34A + LiCl = 14, G34D + NaCl = 14, and G34D + LiCl = 13. Two-way ANOVA with the Tukey test, $^{*}P < 0.05$ and $^{***}P < 0.001$. n.s. indicates no significant difference). (*C*) Representative immunoblots and summary graphs of normalized δ-catenin and GSK3β levels in SH-SY5Y cell lysates transfected with WT or G34S δ-catenin and treated with scrambled (CTRL) (−) or GSK3β (+) siRNA (n = number of immunoblots from three independent cultures. For δ-catenin, G34A + CTRL siRNA = 11, G34A + GSK3β siRNA = 11, G34D + CTRL siRNA = 11, and G34D + GSK3β siRNA = 8. For GSK3β, G34A + CTRL siRNA = 12, G34A + GSK3β siRNA = 10, G34D + CTRL siRNA = 12, and G34D + GSK3β siRNA = 8. Two-way ANOVA with the Tukey test, $^{*}P < 0.05$, $^{**}P < 0.01$, and $^{****}P < 0.0001$. n.s. indicates no significant difference). The position of molecular mass markers (kDa) is shown on the right of the blots. Mean ± SD.

We then examined if lithium-based pharmacological inhibition of in vivo GSK3β activity reversed the δ-catenin G34S mutation's effects on synaptic δ-catenin and AMPAR levels in the cortex. For lithium treatment, we fed 3-mo-old female and male WT and δ-catenin G34S mice with standard chow containing 0.17% w/w lithium carbonate ad libitum for 7 d, a protocol previously shown to significantly inhibit GSK3β activity and elevate δ-catenin levels in the brain (29). After treatment, whole-tissue lysates were collected from the cortex, and pGSK3β levels were measured to assess whether GSK3β activity was inhibited. As expected, in the male and female δ-catenin G34S cortex, lithium treatment significantly increased pGSK3β, when compared to mice fed with standard chow (WT female + standard chow, 1.000 ± 0.311 and WT female + lithium chow, 1.495 ± 0.292, $P = 0.0175$, G34S female + standard chow, 1.024 ± 0.200 and G34S female + lithium chow, 1.481 ± 0.551, $P = 0.0222$, WT male + standard chow, 1.000 ± 0.118 and WT male + lithium chow, 1.455 ± 0.355, $P = 0.0087$, and G34S male + standard chow, 0.931 ± 0.347 and G34S male + lithium chow, 1.347 ± 0.314, $P = 0.0006$), confirming the reduction of in vivo GSK3β activity (*SI Appendix*, Fig. S6 *A* and *B*). Next, the PSD fractions of the cortex were collected from 3-mo-old female and male WT and δ-catenin G34S animals after lithium treatment to determine whether the pharmacological reduction of GSK3β activity increased synaptic δ-catenin and GluA2 levels using immunoblotting. We found that lithium treatment significantly elevated synaptic δ-catenin (WT female + lithium chow, 1.578 ± 0.611, $P = 0.0189$, G34S female + lithium chow, 0.977 ± 0.414, $P = 0.0088$, WT male + lithium chow, 1.929 ± 0.699, $P < 0.0001$, and G34S male + lithium chow, 2.350 ± 0.734, $P < 0.0001$) and GluA2 levels (WT female + lithium chow, 1.705 ± 0.431, $P < 0.0001$, G34S female + lithium chow, 1.432 ± 0.693, $P < 0.0001$, WT male + lithium chow, 1.588 ± 0.476, $P = 0.0016$, and G34S male + lithium chow, 1.795 ± 0.714, $P < 0.0001$) in the mutant female and male cortices compared to those before lithium (Fig. 3 *A* and *B*). However, we found no difference in GluA1 levels (WT female + lithium chow, 1.232 ± 0.731, $P = 0.7081$, G34S female + lithium chow, 0.926 ± 0.587, $P = 0.8723$, WT male + lithium chow, 1.078 ± 0.355, $P = 0.7834$, and G34S male + lithium chow, 1.116 ± 0.515, $P = 0.0539$) between the WT and G34S cortex following lithium treatment (Fig. 3 *A* and *B*). Our findings indicate that the pharmacological inhibition of GSK3β activity significantly elevates synaptic δ-catenin and GluA2 levels in the G34S mutant cortex.

Altered Glutamatergic Activity in Cultured δ-Catenin G34S Cortical Neurons. Certain types of ASD may be caused by a decrease in the signal-to-noise ratio in important brain circuits, which is potentially brought on by changes in a neuronal excitation and inhibition (E/I) balance (57). In fact, maintaining the proper balance of cellular E/I is essential to ensure normal social behavior (13). Moreover, postsynaptic glutamatergic activity in cortical excitatory or inhibitory neurons controls social behavior via the regulation of neuronal E/I within the cortical neural network (13, 19). Consistently, a recent study shows that δ-catenin deficiency increases the E/I ratio and intrinsic excitability in young cortical excitatory cells (31). Given that GluA2 levels are significantly reduced in the δ-catenin G34S cortex (Fig. 3 *A* and *B*), we carried out Ca^{2+} imaging with glutamate uncaging in cultured primary WT and δ-catenin G34S mouse cortical neurons to determine whether the δ-catenin G34S mutation altered glutamatergic activity in excitatory and inhibitory cortical cells. Glutamatergic activity was significantly increased in cultured 12 to 14 days in vitro (DIV) mouse excitatory cortical δ-catenin G34S neurons compared to WT cells (WT, 1.000 ± 0.340 $\Delta F/F_0$ and G34S, 1.307 ± 0.465 $\Delta F/F_0$, $P < 0.0001$) (Fig. 3*C*). Conversely, glutamatergic activity in cultured G34S inhibitory interneurons was markedly lower compared to WT cells (WT, 1.000 ± 0.504 $\Delta F/F_0$ and G34S, 0.621 ± 0.360 $\Delta F/F_0$, $P = 0.0005$) (Fig. 3*D*). In addition to glutamate uncaging, we carried out whole-cell patch-clamp recordings in cultured cortical WT and δ-catenin G34S excitatory and inhibitory cells to directly measure AMPAR-mediated synaptic activity. AMPAR-mediated miniature excitatory postsynaptic currents (mEPSCs) were recorded in DIV 14 to 16 cortical neurons. In consistent with the findings in Ca^{2+} imaging with glutamate uncaging (Fig. 3 *C* and *D*), we found that the average amplitude (WT, 11.78 ± 3.26 pA and G34S, 13.51 ± 2.84 pA, $P = 0.0387$) and

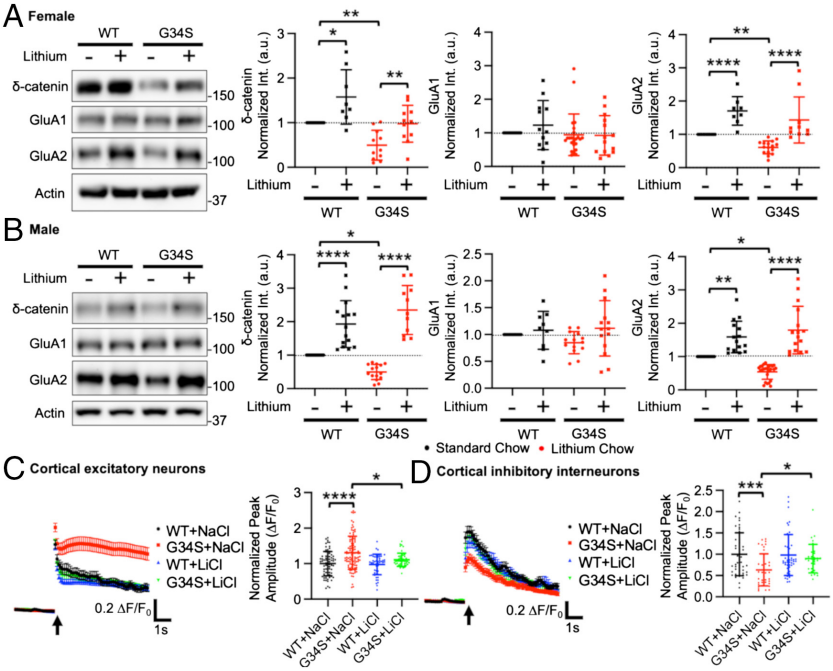

Fig. 3. Lithium treatment reverses a significant reduction of synaptic δ-catenin and GluA2 in the δ-catenin G34S cortex and alterations in glutamatergic activity in cultured cortical neurons. Representative immunoblots and summary graphs of normalized δ-catenin, GluA1, and GluA2 levels in the cortical PSD fractions from standard chow (−) or lithium chow (+)-fed WT and δ-catenin G34S (*A*) female (n = number of immunoblots [number of mice]. For δ-catenin, WT + standard chow =14 [5], WT + lithium chow = 8 [5], G34S + standard chow = 11 [6], and G34S + lithium chow = 11 [6]. For GluA1, WT + standard chow = 14 [5], WT + lithium chow = 12 [5], G34S + standard chow = 23 [6], and G34S + lithium chow = 14 [6]. For GluA2, WT + standard chow = 11 [5], WT + lithium chow = 8 [5], G34S + standard chow = 16 [6], and G34S + lithium chow = 10 [6]) and (*B*) male mice (n = number of immunoblots [number of mice]. For δ-catenin, WT + standard chow = 17 [5], WT + lithium chow = 15 [5], G34S + standard chow = 15 [6], and G34S + lithium chow = 11 [6]. For GluA1, WT + standard chow = 14 [5], WT + lithium chow = 9 [5], G34S + standard chow = 14 [6], and G34S + lithium chow = 14 [6]. For GluA2, WT + standard chow = 18 [5], WT + lithium chow = 15 [5], G34S + standard chow = 24 [6], and G34S + lithium chow = 15 [6], $*P < 0.05$, $**P < 0.01$, and $****P < 0.0001$, Two-way ANOVA with the Tukey test). The position of molecular mass markers (kDa) is shown on the right of the blots. (*C*) Average traces of GCaMP7s signals and summary data of normalized peak amplitude in each condition in excitatory neurons (n = number of neurons from three independent cultures, WT + NaCl = 75, G34S + NaCl = 98, WT + LiCl = 50, and G34S + LiCl = 49). (*D*) Average traces of GCaMP6f signals and summary data of normalized peak amplitude in each condition in inhibitory interneurons (n = number of neurons from 3 independent cultures, WT + NaCl = 46, G34S + NaCl = 40, WT + LiCl = 46, and G34S + LiCl = 31, $*P < 0.05$, $***P < 0.01$, and $****P < 0.0001$, Two-way ANOVA with the Tukey test). An arrow indicates photostimulation. Mean ± SD.

frequency (WT, 2.773 ± 1.080 Hz and G34S, 3.913 ± 0.841 Hz, $P < 0.0001$) of mEPSCs were significantly higher in δ-catenin G34S excitatory neurons compared to WT cells (*SI Appendix*, Fig. S7*A*). Conversely, there was a significantly decrease in the average mEPSC amplitude in δ-catenin G34S inhibitory interneurons compared to WT cells (WT, 76.34 ± 28.64 pA and G34S, 62.61 ± 18.87 pA, $P = 0.0493$), while no significant difference in the average mEPSC frequency was found between WT and KO inhibitory interneurons (WT, 22.84 ± 9.84 Hz and G34S, 18.68 ± 8.68 Hz, $P = 0.1179$) (*SI Appendix*, Fig. S7*B*). These results indicate that the δ-catenin G34S mutation has the opposite effects on glutamatergic AMPAR activity in cortical excitatory and inhibitory cells. Because pharmacological inhibition of GSK3β activity restores normal synaptic expression of δ-catenin and GluA2 in the cortex (Fig. 3 *A* and *B*), we further investigated whether lithium treatment was able to reverse changes in glutamatergic activity in mutant neurons. We treated cultured neurons with 2 mM LiCl for 4 h then performed Ca^{2+} imaging with glutamate uncaging. Pharmacological inhibition of GSK3β activity reversed the δ-catenin G34S effects on glutamatergic activity in cultured cortical excitatory (G34S, 1.109 ± 0.188 $\Delta F/F_0$, $P = 0.0109$) and inhibitory cells (G34S, 0.898 ± 0.334 $\Delta F/F_0$, $P < 0.0419$) (Fig. 3 *C* and *D*). However, lithium treatment in WT neurons had no effect on glutamatergic activity (Excitatory neurons, WT + LiCl, 0.978 ± 0.290 $\Delta F/F_0$, $P = 0.9869$, and inhibitory interneurons, WT + LiCl, 0.982 ± 0.481 $\Delta F/F_0$, $P = 0.9973$) (Fig. 3 *C* and *D*). Finally, GluA2-lacking, GluA1-containing Ca^{2+}-Permeable AMPA Receptors (CP-AMPARs) have larger single-channel conductance (58). We thus hypothesized that the increased glutamatergic activity in δ-catenin G34S excitatory neurons was mediated by the expression of GluA2-lacking CP-AMPARs. To test this idea, we treated cultured cortical neurons with 20 μM 1-naphthyl acetyl spermine (NASPM), a CP-AMPAR blocker, and carried out Ca^{2+} imaging with glutamate uncaging. NASPM treatment was sufficient to abolish an increase in glutamatergic activity in G34S excitatory neurons, while it had no effect on control cells (CTRL) (CTRL, 1.000 ± 0.345 $\Delta F/F_0$, CTRL + NASPM, 1.066 ± 0.353 $\Delta F/F_0$, G34S, 1.275 ± 0.394 $\Delta F/F_0$, $P = 0.0044$, G34S + NASPM, 0.972 ± 0.328, $P = 0.0004$) (*SI Appendix*, Fig. S8). Taken together, we demonstrate that δ-catenin G34S significantly alters AMPAR-mediated glutamatergic activity in excitatory and inhibitory cells in opposite ways, which likely disrupts the neuronal E/I balance in the cortex. Moreover, we find that these changes in G34S mutant neurons are reversed by pharmacological inhibition of GSK3β.

δ-Catenin G34S Induces Social Dysfunction in Mice, Which Is Reversed by GSK3β Inhibition. A three-chamber test was performed to determine whether the δ-catenin G34S mutation affected social behavior. We identified that WT female and male mice interacted significantly longer with stranger 1 than the novel object during the sociability test, an indication of normal sociability (Fig. 4*A* and *SI Appendix*, Table S1). Conversely, in δ-catenin G34S female and male mice, no significant difference in total interaction time was found between stranger 1 and the novel object (Fig. 4*A* and *SI Appendix*, Table S1). Importantly, social interaction time with stranger 1 in δ-catenin G34S female and male mice was significantly less than WT mice (Fig. 4*A* and *SI Appendix*, Table S1). In the social novelty test, WT mice engaged with stranger 2 for longer than they did with stranger 1, demonstrating normal social novelty preference (Fig. 4*B* and *SI Appendix*, Table S1). However, there was no significant difference in reciprocal sniffing time between stranger 1 and stranger 2 in δ-catenin G34S female and male mice (Fig. 4*B* and *SI Appendix*, Table S1). Crucially, compared to WT mice, social interaction with stranger 2 was markedly lower in both female and male δ-catenin G34S animals (Fig. 4*B* and *SI Appendix*, Table S1). These findings indicate that δ-catenin G34S mice exhibit disrupted sociability and social novelty preference in the three-chamber test.

As lithium treatment significantly reduced GSK3β activity and elevated synaptic δ-catenin and GluA2 expression in the δ-catenin G34S cortex (Fig. 3), we examined whether lithium treatment

could restore normal social behavior in mutant mice using the three-chamber test. In the sociability test, we identified that both WT and δ-catenin G34S female and male mice fed with lithium chow interacted with stranger 1 for significantly longer than they did with the novel object, indicating that reduced GSK3β activity reversed disrupted sociability in δ-catenin G34S mice (Fig. 4*A* and *SI Appendix*, Table S1). Furthermore, we found that lithium treatment significantly increased social interaction time with stranger 1 in δ-catenin G34S mice in the sociability test compared to those before lithium (Fig. 4*A* and *SI Appendix*, Table S1). The discrimination index further confirmed that lithium treatment reversed impaired sociability in δ-catenin G34S female and male mice (Fig. 4*A* and *SI Appendix*, Table S2). We also revealed that lithium-fed WT and δ-catenin G34S female and male mice interacted significantly longer with stranger 2 than stranger 1 during the social novelty test, showing that lithium treatment restored normal social novelty preference in δ-catenin G34S mice (Fig. 4*B* and *SI Appendix*, Table S1). In addition, social interaction with stranger 2 in δ-catenin G34S mice was significantly elevated following lithium treatment in the social novelty test compared to those before lithium (Fig. 4*B* and *SI Appendix*, Table S1). Finally, the discrimination index confirmed that lithium treatment restored normal social novelty preference behavior in δ-catenin G34S female and male mice (Fig. 4*B* and *SI Appendix*, Table S2). Taken all together, δ-catenin G34S disrupts social behavior in mice, which is reversed by lithium-based pharmacological inhibition of in vivo GSK3β activity.

δ-Catenin G34S Mice Show Normal Olfaction, Anxiety Levels, and Locomotor Activity. It is possible that sensory deficits may affect performances in social behavioral assays (59). During social activity, mice substantially rely on olfaction (59). The buried food test is a reliable method that depends on the mouse's natural desire to forage using olfactory cues (60). Thus, we conducted the buried food test to examine whether the δ-catenin G34S mutation affected olfactory functions. We found no significant difference in the latency to find the buried food in δ-catenin G34S female and male mice compared to WT littermates (*SI Appendix*, Fig. S9*A* and Table S3), suggesting that δ-catenin G34S mice have normal olfaction. Anxiety levels can also affect social behavior in animals (61, 62). We thus measured locomotor activity and anxiety-like behavior using the open-field test. We found no difference between genotype groups regardless of sex in total traveled distance (locomotor activity) and time spent outside and inside (anxiety-like behavior) (*SI Appendix*, Fig. S9*B* and Table S3). This indicates that δ-catenin G34S mice have normal locomotor activity and anxiety levels, whereby the altered behaviors observed in the three-chamber test (Fig. 4 *A* and *B*) strongly imply social dysfunction.

A Significant Reduction of Synaptic GluA2 in the δ-Catenin KO Cortex and Altered Glutamatergic Activity in Cultured δ-Catenin KO Cortical Neurons. We additionally generated δ-catenin KO mice to further confirm whether the loss of δ-catenin functions was important for glutamatergic activity in cortical neurons and social behavior in animals. We examined if δ-catenin KO affected synaptic AMPAR levels in the brain. First, we confirmed via immunoblotting that there was no δ-catenin expression found in the cortex and hippocampus of δ-catenin KO female and male mice (Fig. 5 *A* and *B* and *SI Appendix*, Fig. S5*B*). The PSD fractions of the cortex were collected from 3-month-old female and male WT and KO animals to analyze for synaptic AMPAR levels as shown in Fig. 3 *A* and *B*. When compared to the WT cortex, we found no difference in synaptic GluA1 levels (WT female, 1.000 and KO female, 1.074 ± 0.268, $P = 0.9426$, and WT male, 1.000 and KO male, 0.996 ± 0.089, $P = 0.8290$) but a significant reduction in GluA2 levels (WT female, 1.000 and KO female, 0.757 ± 0.206, $P = 0.0256$, and WT male, 1.000 and KO male, 0.754 ± 0.187, $P = 0.0175$) in the female and male KO animals' cortices (Fig. 5 *A* and *B*), as seen in the G34S mouse cortex (Fig. 3 *A* and *B*). Next, the PSD fractions of the hippocampus were collected from 3-mo-old female and male WT and δ-catenin KO mice and analyzed for synaptic AMPAR levels using immunoblotting. Like the δ-catenin G34S hippocampus, we found no difference in synaptic GluA1 (WT female, 1.000 and KO female, 0.895 ± 0.092, $P = 0.1870$, and WT male, 1.000 and KO male, 0.866 ± 0.086, $P = 0.8050$) and GluA2 levels (WT female, 1.000 and KO female, 0.9929 ±

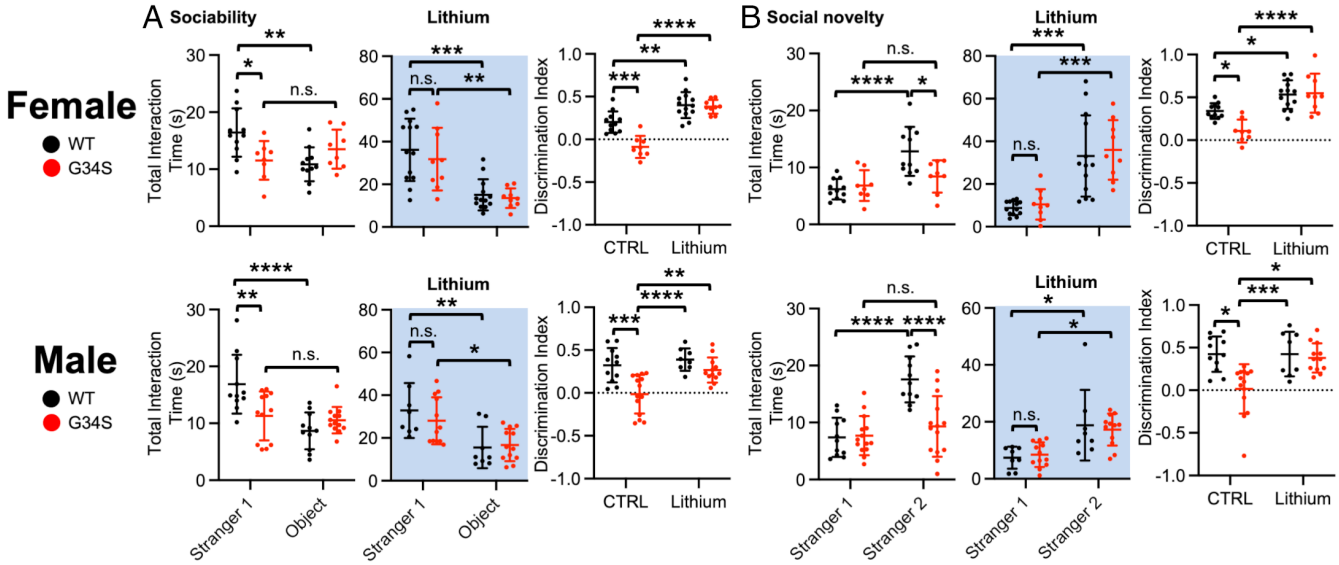

Fig. 4. δ-catenin G34S induces social dysfunction in mice, which is reversed by GSK3β inhibition. Total interaction time and the discrimination index of (*A*) sociability and (*B*) social novelty in female and male mice in each genotype in control and lithium treated conditions (highlighted in light blue) in the three-chamber test (n = number of animals, WT female + standard chow = 11, WT female + lithium chow = 9, G34S female + standard chow = 8, G34S female + lithium chow = 7, WT male + standard chow =11, WT male + lithium chow = 8, G34S male + standard chow = 14, and G34S male + lithium chow = 12, *$P < 0.05$, **$P < 0.01$, ***$P < 0.001$, and ****$P < 0.0001$, Two-way ANOVA with Tukey test. n.s. indicates no significant difference). Mean ± SD.

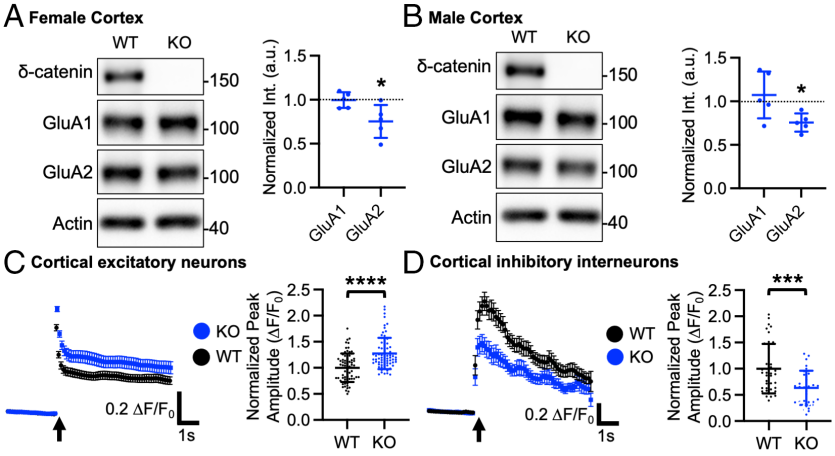

Fig. 5. A significant reduction of synaptic GluA2 in the δ-catenin KO cortex and altered glutamatergic activity in cultured δ-catenin KO cortical neurons. Representative immunoblots and summary graphs of normalized GluA1 and GluA2 levels in the cortical PSD fractions from WT and δ-catenin KO (*A*) female and (*B*) male mice (n = 5 immunoblots from 3 mice in each condition, Kruskal-Wallis test with Dunn's test, $*P < 0.05$). The position of molecular mass markers (kDa) is shown on the right of the blots. (*C*) Average traces of GCaMP7s signals and summary data of normalized peak amplitude in each condition in excitatory neurons (n = number of neurons from 3 independent cultures, WT = 70 and KO = 73). (*D*) Average traces of GCaMP6f signals and summary data of normalized peak amplitude in each condition in inhibitory interneurons (n = number of neurons from three independent cultures, WT = 38 and KO = 30, $***P < 0.01$ and $****P < 0.0001$, the unpaired two-tailed Student's *t* test). An arrow indicates photostimulation. Mean ± SD.

0.119, $P = 0.1134$, and WT male, 1.000 and KO male, 0.882 ± 0.103, $p = 0.1860$) between the WT and KO hippocampus (*SI Appendix*, Fig. S5*B*). This suggests that the loss of δ-catenin expression in mice significantly reduces synaptic GluA2 levels selectively in the cortex, but not in the hippocampus, which likely alters AMPAR-mediated glutamatergic activity in the δ-catenin KO cortex, like the G34S cortex. With this, we conducted Ca^{2+} imaging with glutamate uncaging in cultured WT and δ-catenin KO mouse cortical neurons to determine whether δ-catenin KO altered glutamatergic activity in excitatory and inhibitory cortical neurons as shown in Fig. 3 *C* and *D*. Glutamate-induced Ca^{2+} activity was markedly elevated in cultured 12 to 14 DIV mouse excitatory cortical δ-catenin KO neurons compared to WT cells (WT, 1.000 ± 0.274 $\Delta F/F_0$ and KO, 1.275 ± 0.230 $\Delta F/F_0$, $P < 0.0001$) (Fig. 5*C*). Conversely, glutamatergic activity in cultured KO inhibitory interneurons was significantly lower than WT cells (WT, 1.000 ± 0.0.472 $\Delta F/F_0$ and KO, 0.635 ± 0.327 $\Delta F/F_0$, $P = 0.0005$) (Fig. 5*D*). This suggests that glutamatergic activity in δ-catenin KO excitatory and inhibitory cells is altered in opposite ways, as seen in G34S cortical neurons (Fig. 3 *C* and *D*).

Abnormal Social Behavior but Normal Olfaction, Locomotor Activity, and Anxiety Levels in δ-Catenin KO mice. We used the three-chamber test to determine whether the loss of δ-catenin expression affected social behavior in mice. In the sociability test, WT female and male mice interacted significantly longer with stranger 1 than a novel object, showing normal sociability (Fig. 6*A* and *SI Appendix*, Table S4). However, in δ-catenin KO female and male mice, no significant difference in total interaction time was found between stranger 1 and the novel object (Fig. 6*A* and *SI Appendix*, Table S4). Importantly, social interaction with stranger 1 in δ-catenin KO female and male mice was markedly lower than WT mice (Fig. 6*A* and *SI Appendix*, Table S4). In the social novelty test, WT mice interacted with stranger 2 for longer than they did with stranger 1, an indication of normal social novelty preference (Fig. 6*B* and *SI Appendix*, Table S4). Conversely, there was no significant difference in reciprocal sniffing time between stranger 1 and stranger 2 in δ-catenin KO female and male mice (Fig. 6*B* and *SI Appendix*, Table S4). Compared to WT animals, social interaction with stranger 2 was significantly lower in both female and male δ-catenin KO mice (Fig. 6*B* and *SI Appendix*, Table S4). Moreover, the discrimination index confirmed that δ-catenin KO disrupted social behavior in female and male mice (Fig. 6 *A* and *B* and *SI Appendix*, Table S5). These findings indicate that δ-catenin KO mice exhibit abnormal sociability and social novelty preference in the three-chamber test like δ-catenin G34S mice. In addition, we found that δ-catenin KO female and male mice showed normal olfactory function in the buried food test (*SI Appendix*, Fig. S9*C* and Table S3). Finally, the open-field test showed normal locomotor activity and anxiety levels in δ-catenin KO female and male mice (*SI Appendix*, Fig. S9*D* and Table S3). Altogether, we conclude that δ-catenin KO mice exhibit abnormal social behavior in the three-chamber test without altered olfaction, locomotor activity, and anxiety-like behavior.

δ-Catenin Is Required for Lithium-Induced Restoration of Normal Social Behavior in G34S Mice. Lastly, we used δ-catenin KO mice to address whether δ-catenin was required for lithium effects on social behavior. We fed δ-catenin KO mice with lithium chow and conducted the three-chamber test and compared their social behavior to that of lithium-treated δ-catenin G34S animals. In the sociability test, we found no significant difference in total interaction time between stranger 1 and the novel object in lithium-treated δ-catenin KO female and male mice, an indication of abnormal sociability, whereas we found normal sociability in lithium-treated δ-catenin G34S animals (Fig. 7*A* and *SI Appendix*, Table S6). Importantly, social interaction with stranger 1 in δ-catenin KO female and male mice was markedly lower than G34S mice following lithium treatment (Fig. 7*A* and *SI Appendix*, Table S6). In the social novelty test, after lithium was administered, there was no significant difference in reciprocal sniffing time between stranger 1 and stranger 2 in δ-catenin KO female and male mice, an indication of abnormal social novelty preference, while G34S female and male animals exhibited normal social novelty preference following lithium treatment (Fig. 7*B* and *SI Appendix*, Table S6). Finally, the discrimination index revealed that lithium was unable to restore normal sociability and social novelty preference in δ-catenin KO female and male mice unlike δ-catenin G34S animals (Fig. 7 *A* and *B* and *SI Appendix*, Table S7). These findings suggest that δ-catenin is required for lithium-induced restoration of normal social behavior in δ-catenin G34S mice.

Discussion

ASD is a multifactorial neurodevelopmental disorder characterized by impaired social communication, social interaction, and repetitive behaviors (63). The pathophysiology of ASD is largely influenced by strong genetic components throughout the early stages of development (63). The Simmons Foundation Autism Research Initiative (SFARI) gene database (https://gene.sfari.org) reports more than 1,000 candidate genes and copy number variations (CNVs) loci associated with ASD. Many of these ASD candidate genes are implicated in synaptic formation and function (64).

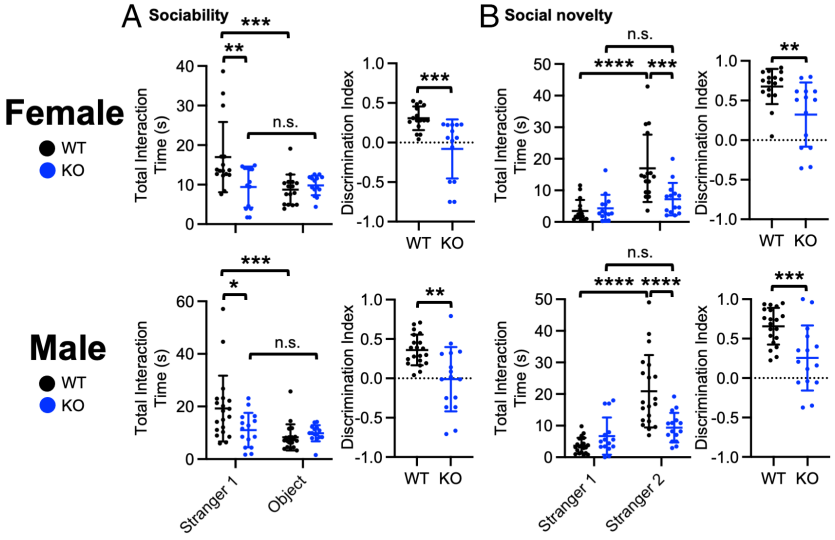

Fig. 6. δ-catenin KO induces social dysfunction in mice. Total interaction time and the discrimination index of (*A*) sociability and (*B*) social novelty in female and male WT and KO mice in the three-chamber test (n = number of animals, WT female = 16, KO female = 14, WT male = 20, and KO male = 15, **P* < 0.05, ***P* < 0.01, ****P* < 0.001, and *****P* < 0.0001, For total interaction time, Two-way ANOVA with Tukey test was used. For the discrimination index, the unpaired two-tailed Student's *t* test was used. n.s. indicates no significant difference). Mean ± SD. Total interaction time and the discrimination index of (*A*) sociability and (*B*) social novelty in female and male WT and KO mice in the three-chamber test (n = number of animals, WT female = 16, KO female = 14, WT male = 20, and KO male = 15, **P* < 0.05, ***P* < 0.01, ****P* < 0.001, and *****P* < 0.0001, For total interaction time, Two-way ANOVA with Tukey test was used. For the discrimination index, the unpaired two-tailed Student's *t* test was used. n.s. indicates no significant difference). Mean ± SD.

In fact, several molecular, cellular, and functional studies of ASD experimental models suggest that synaptic abnormalities underlie ASD pathogenesis (known as synaptopathy) (65). However, the mechanisms by which these gene products induce synaptopathy and ASD symptoms are not completely understood. The *δ-catenin* gene is strongly associated with ASD according to multiple human genetic studies (20–24). Notably, the ASD-associated G34S mutation in the *δ-catenin* gene induces a loss of δ-catenin functions in excitatory synapses (24). However, how the ASD-associated δ-catenin missense mutation causes the loss of δ-catenin functions to contribute to ASD synaptopathy remains unclear. Here, we use neuroblastoma cells to identify that the ASD-associated δ-catenin G34S mutation enhances δ-catenin degradation, which is completely reversed by the reduction of GSK3β activity. Additionally, using two mouse models, δ-catenin G34S knockin and δ-catenin KO, we further identify that the δ-catenin deficiency alters cortical glutamatergic E/I at the cellular levels and disrupts social behavior. Moreover, pharmacological inhibition of GSK3β activity can reverse δ-catenin G34S-induced abnormal glutamatergic E/I and social deficits. Finally, we show that δ-catenin is required for lithium-induced restoration of normal social behavior in δ-catenin G34S mice. As the expression of δ-catenin is highly correlated with other ASD-risk genes that are involved in synaptic structure and function (31, 36–38), our findings can help us to better understand ASD synaptopathy.

In the previous works addressing a loss of δ-catenin functions, two mouse lines of δ-catenin deficiency were used. The first known mouse model contains a truncated form of δ-catenin protein (δ-catenin N-term mice) (35), making it unable to address comprehensive loss-of-function effects. Furthermore, these mice have not been used to investigate the role of δ-catenin in social behavior. The second mouse model that has disruption in the *δ-catenin* gene has showed impaired social behavior (66). The study, however, has not confirmed that δ-catenin protein expression is completely absent. Furthermore, this study exclusively used male mice, obviating the possibility of addressing sex disparities, which are common in many mental illnesses that are accompanied by social dysfunction (67). In contrast, we examine female and male mice separately and finds that our δ-catenin KO female and male mice contain no full-length or truncated δ-catenin protein expression (Fig. 5 *A* and *B* and *SI Appendix*. Figs. S5*B* and S11*C*) and exhibit social dysfunction (Fig. 6 *A* and *B*). Therefore, employing δ-catenin G34S knockin and δ-catenin KO mouse lines allows us to examine the δ-catenin-mediated neural mechanisms underlying social behavior in greater detail.

We show that the loss of δ-catenin functions in the G34S mutation and KO has similar opposing effects on glutamatergic activity in cortical excitatory and inhibitory cells (Figs. 3 *C* and *D* and 5 *C* and *D*). We further demonstrate that G34S neurons exhibit thesame pattern of alteration in AMPAR-mediated mEPSCs (*SI Appendix*, Fig. S6 *A* and *B*). However, it remains unclear how the loss of δ-catenin functions differentially affects cellular excitation and inhibition. GluA2-containing AMPARs are Ca^{2+} impermeable, whereas GluA2-lacking AMPARs are Ca^{2+} permeable and have high single channel conductance (58). Cortical excitatory neurons have no basal Ca^{2+}-permeable AMPAR expression, while cortical inhibitory interneurons contain GluA2-lacking CP-AMPARs (68). Therefore, δ-catenin G34S and KO-induced reduction of GluA2 in excitatory cells may promote the synaptic expression of highly conductive GluA2-lacking Ca^{2+}-permeable AMPARs, which contributes to higher glutamatergic and neuronal activity. In fact, we identify that increased glutamatergic activity measured by Ca^{2+} imaging with glutamate uncaging in δ-catenin G34S excitatory cells is significantly decreased when we treat with the CP-AMPAR blocker, NASPM (*SI Appendix*, Fig. S8), which supports our idea. Conversely, in δ-catenin G34S and KO inhibitory interneurons, GluA1/2 or GluA2/3 heteromeric AMPARs are likely decreased, which leads to an overall decrease in glutamatergic and neuronal activity. Research suggests that GluA2 is expressed in most cortical inhibitory interneurons, which is likely affected by δ-catenin deficiency in our study, although it is considerably lower in cortical interneurons than pyramidal neurons (69–73).This suggests that while δ-catenin deficiency lowers synaptic GluA2 levels in cortical neurons, it has the opposite effects on glutamatergic and neuronal activity in excitatory and inhibitory cells, potentially altering the E/I balance. Alternatively, extrasynaptic glutamatergic receptors may play important roles in altered glutamatergic activity in δ-catenin G34S cells. Several extrasynaptic AMPARs and NMDA receptors (NMRARs) are expressed on the plasma membrane of neurons, and it is known that these receptors function differently from those directed at the PSD (74). Specifically, a small number of CP-AMPARs are in extrasynaptic area where they can be rapidly recruited to synapses during synaptic plasticity (75, 76). Therefore, it is possible that δ-catenin deficiency affects glutamatergic activity via these receptor populations. Another explanation is that the loss of synaptic GluA2 leads to a reduction of excitability in δ-catenin deficiency inhibitory neurons, which results in less synaptic inhibition in glutamatergic neurons and thus an increase of neuronal activity in these cells (disinhibition). Notably, a recent study

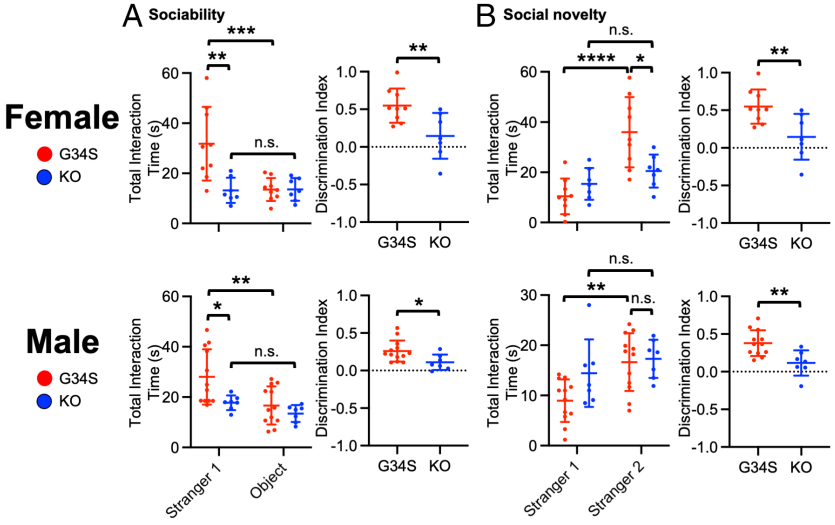

Fig. 7. δ-catenin is required for lithium-induced restoration of normal social behavior in G34S mice. Total interaction time and the discrimination index of (*A*) sociability and (*B*) social novelty in lithium-treated female and male G34S and KO mice in the three-chamber test (n = number of animals, G34S female + lithium = 9, KO female + lithium = 7, G34S male + lithium = 12, and KO male + lithium = 7, **P* < 0.05, ***P* < 0.01, ****P* < 0.001, and *****P* < 0.0001, For total interaction time, Two-way ANOVA with Tukey test was used. For the discrimination index, the unpaired two-tailed Student's *t* test was used. n.s. indicates no significant difference). Mean ± SD.

shows that the loss of δ-catenin functions induced by shRNA-mediated δ-catenin knockdown significantly decreases cortical neurons' inhibition to increase excitation (31). Research also suggests that parvalbumin-positive (PV+) inhibitory interneurons in the medial prefrontal cortex (mPFC) receive direct glutamatergic inputs from the ventral hippocampus, mediodorsal thalamus, and basolateral amygdala to drive feedforward inhibition onto prefrontal pyramidal neurons, which is important for the regulation of social behavior (6, 7, 10, 77–79). Hence, δ-catenin may be important for glutamatergic activity in PV+ inhibitory interneurons to provide feedforward inhibition onto pyramidal neurons in the mPFC, which regulates social behavior. δ-catenin deficiency-induced disinhibition thus could contribute to the increase in neuronal activity in excitatory cells, particularly in the intact circuits, to cause social dysfunction. Finally, a recent study identifies that δ-catenin also localizes to inhibitory synapses (31). Therefore, it is possible that δ-catenin deficiency directly affects inhibitory synapses to change E/I ratio. In conclusion, there are still many important questions surrounding the molecular mechanisms of how δ-catenin deficiency affects E/I ratio.

Pharmacological treatment of ASD is challenging, due in large part to the heterogeneity in the presentation of ASD (80). Existing therapies aim to treat specific symptoms, rather than address the basic underlying etiologies (81). Thus, areas of research focusing on therapeutic agents that directly target the underlying pathology of ASD are an important current and future need. Recent studies suggest that GSK3β activity is strongly implicated in the pathophysiology of ASD (39–46). However, extensive studies have yielded inconsistent data on the role of GSK3β activity in the molecular and behavioral effects. For example, elevated GSK3β activity is responsible for the ASD-related phenotypes in the mouse model of fragile X mental retardation (FMR) (39–42). Conversely, inactivation of GSK3β is associated with the ASD-related phenotypes found in deletion of the *phosphatase and tensin homolog on chromosome ten (PTEN)* gene in mice (43). Nonetheless, our study identifies GSK3β as the target to complete the synaptic δ-catenin regulatory pathway and recognizes GSK3β as a therapeutic target for limiting the loss of δ-catenin function-induced synaptopathy in ASD. Moreover, we use lithium to demonstrate inhibition of GSK3β activity as a therapeutic target. Lithium reduces GSK3β activity by elevating the Akt-dependent phosphorylation of the GSK3β autoinhibitory residue, serine 9 (82) or by competing with magnesium for enzyme binding (83). Interestingly, there is strong evidence that lithium acts as a mood stabilizer through inhibition of GSK3β (84, 85). Furthermore, one therapeutic action of lithium is the ability to regulate protein stability, in particular synaptic proteins (47, 86). Significantly, we have previously reported that lithium reduces GSK3β activity and stabilizes synaptic δ-catenin, thus elevating the δ-catenin complex consisting of AMPARs and synaptic activity in hippocampal synapses (29). Moreover, the current study demonstrates that lithium can elevate synaptic δ-catenin and GluA2 levels in the cortex and enhance social behavior in mice, which requires δ-catenin expression. Indeed, lithium administration to 30 children and adolescents diagnosed with ASD was shown to improve the symptoms in 43% of patients (87). Therefore, an increase in δ-catenin levels at synapses by the reduction of GSK3β activity stabilizes synaptic AMPARs and spine integrity, which could be beneficial for ASD. Therefore, our work further allows us to test a clinically applicable therapeutic protocol for ASD.

Additional interesting findings in our study show that total δ-catenin and GluA2 levels were significantly lower in the male G34S cortex compared to the male WT cortex, while there were no differences in total δ-catenin and GluA2 levels between the female WT and G34S cortex (*SI Appendix*, Fig. S4). Moreover, lithium treatment restores normal synaptic δ-catenin levels in the female G34S cortex (Fig. 3*A*), while synaptic δ-catenin levels are much higher in the male G34S cortex following lithium (Fig. 3*B*). This suggests that there are potential sex differences in the regulation of total δ-catenin and GluA2 expression. Importantly, studies suggest that δ-catenin and GluA2 levels can be controlled by estrogen signaling (88–90). This indicates that δ-catenin and GluA2 expression may be differentially regulated by the sex of animals, which is an important topic for future research as sex differences in social dysfunction are common (91).

Materials and Methods

Animals. All mice were bred in the animal facility at Colorado State University (CSU). Animals were housed under 12:12 h light/dark cycle. 3-mo-old male and female mice were used in the current study. CSU's Institutional Animal Care and Use Committee reviewed and approved the animal care and protocol (3408). δ-catenin G34S mice (RRID:MMRRC_050621-UCD) were generated by Jyothi Arikkath at UNMC Mouse Genome Engineering Core using the CRISPR-Cas9 technique (54). δ-catenin KO mouse was developed in collaboration with Cyagen Biosciences Inc. utilizing the CRISPR-Cas9 technique (54). Detailed information on generation of δ-catenin G34S and KO mice used in this study are found in *SI Appendix*. Lithium

treatment in animals was conducted as described previously (29). Lithium animals received standard chow containing 0.17% w/w lithium carbonate (Harlan Teklad) ad libitum for 7 d. Control animals were fed with standard chow.

DNA Cloning. pSinRep5-WT δ-catenin and pSinRep5-G34S δ-catenin plasmids were gifts from Dr. Edward Ziff (New York University Langone Health). HA-tagged WT δ-catenin and G34S δ-catenin were cloned into the mammalian expression vector, pcDNA3.1. The QuikChange XL Site-Directed Mutagenesis Kit (Agilent Technologies) was used to generate G34A and G34D mutations from the WT δ-catenin plasmid. The following primers were used with the bolded regions being where the mutations were made to exchange the glycine (GGC): G34A primers 5′-GCTCCTTGAGCCCA***GCC***TTAAACACCTCCAA-3′ and 5′-TTGGAGGTGTTTAAGGCTGGGCTCAAGGAGC-3′, and the G34D primers 5′-CAG CTCCTTGAGCCCA***GAC***TTAAACACCTCCAATG-3′ and 5′-CATTGGAGGTGTTTAAGTCTGGG CTC AAGGAGCTG-3′.

Human Neuroblastoma Cell (SH-SY5Y) Culture and Transfection. SH-SY5Y cells were grown in DMEM medium with fetal bovine serum (Life Technologies) and 1% penicillin/streptomycin (Life Technologies). Totally, 500,000 cells were plated in six-well dishes and 1 μg DNA was transfected when cells reached 75 to 85% confluency with Lipofectamine 2000 (Life Technologies) according to the manufacturer's instructions. Then, 25 nM control siRNA ON-TARGETplus nontargeting pool (Dharmacon siRNA solution) and 25 nM SMARTpool ON-TARGETplus human GSK3β siRNA (Dharmacon siRNA solution) were transfected with 1 μg of DNA when cells reached 50% confluency, and cell lysates were collected 72 h later. Cells used for each experiment were from more than three independently prepared cultures.

Primary Cortical Neuron Culture. Postnatal day 0 (P0) male and female pups from WT, δ-catenin G34S or KO mice were used to produce mouse cortical neuron cultures as shown previously (92, 93). Heterozygous G34S or KO mice were used to breed for generating each genotype. PCR was performed to identify each genotype before preparing cultures.

GCaMP Ca^{2+} Imaging with Glutamate Uncaging. We carried out Ca^{2+} imaging with glutamate uncaging in cultured mouse cortical neurons to determine glutamatergic activity as described previously (94). Detailed information on GCaMP Ca^{2+} imaging with glutamate uncaging used in this study is found in *SI Appendix*.

Animal Behavioral Assays. To determine social behavior, a three-chamber test was performed with a modification of the previously described method (95). The buried food assay was performed as described previously (96). We measured locomotor activity and anxiety-like behavior using the open-field test as carried out previously (95). Detailed information on behavioral tests used in this study is found in *SI Appendix*.

Statistical Analysis. We used the GraphPad Prism 9 software to determine statistical significance (set at $P < 0.05$). Grouped results of single comparisons were tested for normality with the Shapiro–Wilk normality or Kolmogorov–Smirnov test and analyzed using the unpaired two-tailed Student's *t* test when data are normally distributed. Differences between multiple groups were assessed by two-way ANOVA) with the Tukey test or nonparametric Kruskal–Wallis test with Dunn's test. The graphs were presented as mean ± SD.

Other detailed Methods and Materials used in this study are found in *SI Appendix*.

Data, Materials, and Software Availability. All study data are included in the article and/or *SI Appendix*.

ACKNOWLEDGMENTS. We thank members of the Kim laboratory for their generous support. We appreciate thoughtful suggestion from Dr. Edward Ziff. This work is funded by College Research Council Shared Research Program and Student Experiential Learning Grants from CSU, the Jerome Lejeune Foundation, the NIH/NCATS Colorado CTSA Grant (UL1 TR002535), the Boettcher Foundation's Webb-Waring Biomedical Research Program, and the NIH grant (1R03AG072102) for S.K. This work is also supported by the NIH grant (R01MH126017) for S.C. Contents are the authors' sole responsibility and do not necessarily represent official NIH views. This work was prepared while Jyothi Arikkath was employed at the University of Nebraska Medical Center. The opinions expressed in this article are the author's own and do not reflect the views of the NIH, the Department of Health and Human Services, or the United States Government.

Author affiliations: [a]Department of Biomedical Sciences, Colorado State University, Fort Collins, CO 80523; [b]Cellular and Molecular Biology Program, Colorado State University Fort Collins CO 80523; [c]Molecular, Cellular and Integrative Neurosciences Program, Colorado State University, Fort Collins, CO 80523; [d]Department of Biochemistry & Molecular Biology, Colorado State University, Fort Collins, CO 80523; [e]Rocky Mountain High School, Fort Collins, CO 80526; and [f]Developmental Neuroscience, Munore-Meyer Institute, University of Nebraska Medical Center, Omaha, NE 68198

1. J. Ko, Neuroanatomical substrates of rodent social behavior: The medial prefrontal cortex and its projection patterns. *Front. Neural Circuits* **11**, 41 (2017).
2. I. Rapin, R. Katzman, Neurobiology of autism. *Ann Neurol* **43**, 7–14 (1998).
3. R. C. Abrams, L. A. Spielman, G. S. Alexopoulos, E. Klausner, Personality disorder symptoms and functioning in elderly depressed patients. *Am. J. Geriatr Psychiatry* **6**, 24–30 (1998).
4. J. O. Goldberg, L. A. Schmidt, Shyness, sociability, and social dysfunction in schizophrenia. *Schizophr. Res.* **48**, 343–349 (2001).
5. American Psychiatric Association, *Diagnostic and Statistical Manual of Mental Disorders (DSM-5®)* (American Psychiatric Pub, 2013).
6. Q. Sun *et al.*, Ventral hippocampal-prefrontal interaction affects social behavior via parvalbumin positive neurons in the medial prefrontal cortex. *iScience* **23**, 100894 (2020).
7. A. C. Felix-Ortiz, A. Burgos-Robles, N. D. Bhagat, C. A. Leppla, K. M. Tye, Bidirectional modulation of anxiety-related and social behaviors by amygdala projections to the medial prefrontal cortex. *Neuroscience* **321**, 197–209 (2016).
8. J. P. Little, A. G. Carter, Subcellular synaptic connectivity of layer 2 pyramidal neurons in the medial prefrontal cortex. *J. Neurosci.* **32**, 12808–12819 (2012).
9. S. Xu *et al.*, Neural circuits for social interactions: From microcircuits to input-output circuits. *Front. Neural Circuits* **15**, 768294 (2021).
10. B. R. Ferguson, W. J. Gao, Thalamic control of cognition and social behavior via regulation of gamma-aminobutyric acidergic signaling and excitation/inhibition balance in the medial prefrontal cortex. *Biol. Psychiatry* **83**, 657–669 (2018).
11. W. C. Huang, Y. Chen, D. T. Page, Hyperconnectivity of prefrontal cortex to amygdala projections in a mouse model of macrocephaly/autism syndrome. *Nat. Commun.* **7**, 13421 (2016).
12. A. Selimbeyoglu *et al.*, Modulation of prefrontal cortex excitation/inhibition balance rescues social behavior in CNTNAP2-deficient mice. *Sci. Transl. Med.* **9**, eaah6733 (2017).
13. O. Yizhar *et al.*, Neocortical excitation/inhibition balance in information processing and social dysfunction. *Nature* **477**, 171–178 (2011).
14. W. Cao *et al.*, Gamma oscillation dysfunction in mPFC leads to social deficits in neuroligin 3 R451C knockin mice. *Neuron* **97**, 1253–1260.e7 (2018).
15. F. Abell *et al.*, The neuroanatomy of autism: A voxel-based whole brain analysis of structural scans. *Neuroreport* **10**, 1647–1651 (1999).
16. F. Castelli, C. Frith, F. Happe, U. Frith, Autism, Asperger syndrome and brain mechanisms for the attribution of mental states to animated shapes. *Brain* **125**, 1839–1849 (2002).
17. N. Schmitz *et al.*, Neural correlates of executive function in autistic spectrum disorders. *Biol. Psychiatry* **59**, 7–16 (2006).
18. A. C. Brumback *et al.*, Identifying specific prefrontal neurons that contribute to autism-associated abnormalities in physiology and social behavior. *Mol. Psychiatry* **23**, 2078–2089 (2018).
19. L. Liu *et al.*, Cell type-differential modulation of prefrontal cortical GABAergic interneurons on low gamma rhythm and social interaction. *Sci. Adv.* **6**, eaay4073 (2020).
20. I. O. Tuncay *et al.*, Analysis of recent shared ancestry in a familial cohort identifies coding and noncoding autism spectrum disorder variants. *NPJ Genom Med.* **7**, 13 (2022).
21. D. E. Miller, A. Squire, J. T. Bennett, A child with autism, behavioral issues, and dysmorphic features found to have a tandem duplication within CTNND2 by mate-pair sequencing. *Am. J. Med. Genet. A* **182**, 543–547 (2020), 10.1002/ajmg.a.61442.
22. H. Guo *et al.*, Inherited and multiple de novo mutations in autism/developmental delay risk genes suggest a multifactorial model. *Mol. Autism* **9**, 64 (2018).
23. T. Wang *et al.*, De novo genic mutations among a Chinese autism spectrum disorder cohort. *Nat. Commun.* **7**, 13316 (2016).
24. T. N. Turner *et al.*, Loss of delta-catenin function in severe autism. *Nature* **520**, 51–56 (2015).
25. J. B. Silverman *et al.*, Synaptic anchorage of AMPA receptors by cadherins through neural plakophilin-related arm protein AMPA receptor-binding protein complexes. *J. Neurosci.* **27**, 8505–8516 (2007).
26. M. Peifer, S. Berg, A. B. Reynolds, A repeating amino acid motif shared by proteins with diverse cellular roles. *Cell* **76**, 789–791 (1994).
27. M. Takeichi, Cadherins: Key molecules for selective cell-cell adhesion. *IARC Sci. Publ.*, 76–79 (1988).
28. J. Gilbert, H. Y. Man, The X-linked autism protein KIAA2022/KIDLIA regulates neurite outgrowth via N-cadherin and delta-catenin signaling. *eNeuro* **3**, ENEURO.0238-16.2016 (2016).
29. M. Farooq *et al.*, Lithium increases synaptic GluA2 in hippocampal neurons by elevating the delta-catenin protein. *Neuropharmacology* **113**, 426–433 (2016), 10.1016/j.neuropharm.2016.10.025.
30. S. Restituito *et al.*, Synaptic autoregulation by metalloproteases and gamma-secretase. *J. Neurosci.* **31**, 12083–12093 (2011).
31. N. Assendorp, CTNND2 moderates neuronal excitation and links human evolution to prolonged synaptic development in the neocortex. bioRxiv [Preprint] (2022), https://doi.org/10.1101/2022.09.13.507776 (Accessed 14 September 2022).
32. K. S. Kosik, C. P. Donahue, I. Israely, X. Liu, T. Ochiishi, Delta-catenin at the synaptic-adherens junction. *Trends Cell Biol.* **15**, 172–178 (2005).
33. L. Yuan, E. Seong, J. L. Beuscher, J. Arikkath, delta-catenin regulates spine architecture via cadherin and PDZ-dependent interactions. *J. Biol. Chem.* **290**, 10947–10957 (2015).

34. C. Matter, M. Pribadi, X. Liu, J. T. Trachtenberg, Delta-catenin is required for the maintenance of neural structure and function in mature cortex in vivo. *Neuron* **64**, 320–327 (2009).
35. I. Israely *et al.*, Deletion of the neuron-specific protein delta-catenin leads to severe cognitive and synaptic dysfunction. *Curr. Biol.* **14**, 1657–1663 (2004).
36. S. Ramanathan *et al.*, A case of autism with an interstitial deletion on 4q leading to hemizygosity for genes encoding for glutamine and glycine neurotransmitter receptor sub-units (AMPA 2, GLRA3, GLRB) and neuropeptide receptors NPY1R, NPY5R. *BMC Med. Genet.* **5**, 10 (2004).
37. A. El-Amraoui, C. Petit, Cadherins as targets for genetic diseases. *Cold Spring Harb. Perspect. Biol.* **2**, a003095 (2010).
38. R. Mejias *et al.*, Gain-of-function glutamate receptor interacting protein 1 variants alter GluA2 recycling and surface distribution in patients with autism. *Proc. Natl. Acad. Sci. U.S.A.* **108**, 4920–4925 (2011).
39. W. W. Min *et al.*, Elevated glycogen synthase kinase-3 activity in Fragile X mice: Key metabolic regulator with evidence for treatment potential. *Neuropharmacology* **56**, 463–472 (2009).
40. C. J. Yuskaitis *et al.*, Lithium ameliorates altered glycogen synthase kinase-3 and behavior in a mouse model of fragile X syndrome. *Biochem. Pharmacol.* **79**, 632–646 (2010).
41. E. J. McManus *et al.*, Role that phosphorylation of GSK3 plays in insulin and Wnt signalling defined by knockin analysis. *EMBO J.* **24**, 1571–1583 (2005).
42. M. A. Mines, C. J. Yuskaitis, M. K. King, E. Beurel, R. S. Jope, GSK3 influences social preference and anxiety-related behaviors during social interaction in a mouse model of fragile X syndrome and autism. *PLoS One* **5**, e9706 (2010).
43. C. H. Kwon *et al.*, Pten regulates neuronal arborization and social interaction in mice. *Neuron* **50**, 377–388 (2006).
44. Y. Mao *et al.*, Disrupted in schizophrenia 1 regulates neuronal progenitor proliferation via modulation of GSK3beta/beta-catenin signaling. *Cell* **136**, 1017–1031 (2009).
45. W. Y. Kim, W. D. Snider, Functions of GSK-3 signaling in development of the nervous system. *Front Mol. Neurosci.* **4**, 44 (2011).
46. X. Wu *et al.*, Lithium ameliorates autistic-like behaviors induced by neonatal isolation in rats. *Front. Behav. Neurosci.* **8**, 234 (2014).
47. O. O'Leary, Y. Nolan, Glycogen synthase kinase-3 as a therapeutic target for cognitive dysfunction in neuropsychiatric disorders. *CNS Drugs* **29**, 1–15 (2015).
48. S. Bareiss, K. Kim, Q. Lu, Delta-catenin/NPRAP: A new member of the glycogen synthase kinase-3beta signaling complex that promotes beta-catenin turnover in neurons. *J. Neurosci. Res.* **88**, 2350–2363 (2010).
49. M. Oh *et al.*, GSK-3 phosphorylates delta-catenin and negatively regulates its stability via ubiquitination/proteosome-mediated proteolysis. *J. Biol. Chem.* **284**, 28579–28589 (2009).
50. C. Yost *et al.*, The axis-inducing activity, stability, and subcellular distribution of beta-catenin is regulated in Xenopus embryos by glycogen synthase kinase 3. *Genes Dev.* **10**, 1443–1454 (1996).
51. M. Peifer, L. M. Pai, M. Casey, Phosphorylation of the Drosophila adherens junction protein Armadillo: Roles for wingless signal and zeste-white 3 kinase. *Dev. Biol.* **166**, 543–556 (1994).
52. I. Celen, K. E. Ross, C. N. Arighi, C. H. Wu, Bioinformatics knowledge map for analysis of beta-catenin function in cancer. *PLoS One* **10**, e0141773 (2015).
53. Y. Xue *et al.*, GPS 2.0, a tool to predict kinase-specific phosphorylation sites in hierarchy. *Mol. Cell Proteomics* **7**, 1598–1608 (2008).
54. D. W. Harms, Mouse genome editing using the CRISPR/Cas system. *Curr. Protoc Hum. Genet.* **83**, 15.17.1–15.17.27 (2014).
55. N. Chen *et al.*, Interaction proteomics reveals brain region-specific AMPA receptor complexes. *J.Proteome Res.* **13**, 5695–5706 (2014).
56. M. Maheshwari, A. Samanta, S. K. Godavarthi, R. Mukherjee, N. R. Jana, Dysfunction of the ubiquitin ligase Ube3a may be associated with synaptic pathophysiology in a mouse model of Huntington disease. *J. Biol. Chem.* **287**, 29949–29957 (2012).
57. J. L. Rubenstein, M. M. Merzenich, Model of autism: Increased ratio of excitation/inhibition in key neural systems. *Genes Brain Behav.* **2**, 255–267 (2003).
58. G. H. Diering, R. L. Huganir, The AMPA receptor code of synaptic plasticity. *Neuron* **100**, 314–329 (2018).
59. G. K. Beauchamp, K. Yamazaki, Chemical signalling in mice. *Biochem. Soc. Trans.* **31**, 147–151 (2003).
60. M. Yang, J. N. Crawley, Simple behavioral assessment of mouse olfaction. *Curr. Protoc. Neurosci.* **Chapter 8**, Unit 8.24 (2009).
61. A. K. Beery, D. Kaufer, Stress, social behavior, and resilience: Insights from rodents. *Neurobiol. Stress* **1**, 116–127 (2015).
62. M. Yang, J. L. Silverman, J. N. Crawley, Automated three-chambered social approach task for mice. *Curr. Protoc. Neurosci.* Chapter 8, **Unit 8.26** (2011).
63. S. Guang *et al.*, Synaptopathology involved in autism spectrum disorder. *Front. Cell. Neurosci.* **12**, 470 (2018).
64. J. Gilbert, H. Y. Man, Fundamental elements in autism: From neurogenesis and neurite growth to synaptic plasticity. *Front. Cell. Neurosci.* **11**, 359 (2017).
65. H. Won, W. Mah, E. Kim, Autism spectrum disorder causes, mechanisms, and treatments: Focus on neuronal synapses. *Front. Mol. Neurosci.* **6**, 19 (2013).
66. X. Wang *et al.*, Rictor is involved in Ctnnd2 deletion-induced impairment of spatial learning and memory but not autism-like behaviors. *Front. Biosci. (Landmark Ed)* **26**, 335–346 (2021).
67. M. M. Wickens, D. A. Bangasser, L. A. Briand, Sex differences in psychiatric disease: A focus on the glutamate system. *Front. Mol. Neurosci.* **11**, 197 (2018).
68. J. T. Isaac, M. C. Ashby, C. J. McBain, The role of the GluR2 subunit in AMPA receptor function and synaptic plasticity. *Neuron* **54**, 859–871 (2007).
69. J. R. Geiger *et al.*, Relative abundance of subunit mRNAs determines gating and Ca2+ permeability of AMPA receptors in principal neurons and interneurons in rat CNS. *Neuron* **15**, 193–204 (1995).
70. B. Rudy, G. Fishell, S. Lee, J. Hjerling-Leffler, Three groups of interneurons account for nearly 100% of neocortical GABAergic neurons. *Dev. Neurobiol.* **71**, 45–61 (2011).
71. R. N. Kooijmans, M. W. Self, F. G. Wouterlood, J. A. Belien, P. R. Roelfsema, Inhibitory interneuron classes express complementary AMPA-receptor patterns in macaque primary visual cortex. *J. Neurosci.* **34**, 6303–6315 (2014).
72. N. K. Adotevi, B. Leitch, Synaptic changes in AMPA receptor subunit expression in cortical parvalbumin interneurons in the stargazer model of absence epilepsy. *Front. Mol. Neurosci.* **10**, 434 (2017).
73. M. Kondo, R. Sumino, H. Okado, Combinations of AMPA receptor subunit expression in individual cortical neurons correlate with expression of specific calcium-binding proteins. *J. Neurosci.* **17**, 1570–1581 (1997).
74. B. Pal, Involvement of extrasynaptic glutamate in physiological and pathophysiological changes of neuronal excitability. *Cell Mol. Life Sci.* **75**, 2917–2949 (2018).
75. K. He *et al.*, Stabilization of Ca2+-permeable AMPA receptors at perisynaptic sites by GluR1-S845 phosphorylation. *Proc. Natl. Acad. Sci. U.S.A.* **106**, 20033–20038 (2009).
76. J. L. Sanderson *et al.*, AKAP150-anchored calcineurin regulates synaptic plasticity by limiting synaptic incorporation of Ca2+-permeable AMPA receptors. *J. Neurosci.* **32**, 15036–15052 (2012).
77. R. Marek *et al.*, Hippocampus-driven feed-forward inhibition of the prefrontal cortex mediates relapse of extinguished fear. *Nat. Neurosci.* **21**, 384–392 (2018).
78. L. M. McGarry, A. G. Carter, Inhibitory gating of basolateral amygdala inputs to the prefrontal cortex. *J. Neurosci.* **36**, 9391–9406 (2016).
79. K. Delevich, J. Tucciarone, Z. J. Huang, B. Li, The mediodorsal thalamus drives feedforward inhibition in the anterior cingulate cortex via parvalbumin interneurons. *J. Neurosci.* **35**, 5743–5753 (2015).
80. R. E. Accordino, C. Kidd, L. C. Politte, C. A. Henry, C. J. McDougle, Psychopharmacological interventions in autism spectrum disorder. *Expert Opin. Pharmacother.* **17**, 937–952 (2016).
81. D. R. Hampson, S. Gholizadeh, L. K. Pacey, Pathways to drug development for autism spectrum disorders. *Clin. Pharmacol. Ther.* **91**, 189–200 (2012).
82. F. Zhang, C. J. Phiel, L. Spece, N. Gurvich, P. S. Klein, Inhibitory phosphorylation of glycogen synthase kinase-3 (GSK-3) in response to lithium. Evidence for autoregulation of GSK-3. *J. Biol. Chem.* **278**, 33067–33077 (2003).
83. W. J. Ryves, A. J. Harwood, Lithium inhibits glycogen synthase kinase-3 by competition for magnesium. *Biochem. Biophys. Res. Commun.* **280**, 720–725 (2001).
84. W. T. O'Brien, P. S. Klein, Validating GSK3 as an in vivo target of lithium action. *Biochem. Soc. Trans.* **37**, 1133–1138 (2009).
85. D. M. Chuang, H. K. Manji, In search of the Holy Grail for the treatment of neurodegenerative disorders: Has a simple cation been overlooked? *Biol. Psychiatry* **62**, 4–6 (2007).
86. C. Xu, N. G. Kim, B. M. Gumbiner, Regulation of protein stability by GSK3 mediated phosphorylation. *Cell Cycle* **8**, 4032–4039 (2009).
87. M. Siegel *et al.*, Preliminary investigation of lithium for mood disorder symptoms in children and adolescents with autism spectrum disorder. *J. Child Adolesc. Psychopharmacol.* **24**, 399–402 (2014).
88. G. V. Raj *et al.*, Estrogen receptor coregulator binding modulators (ERXs) effectively target estrogen receptor positive human breast cancers. *Elife* **6**, e26857 (2017).
89. J. A. Avila *et al.*, Estradiol rapidly increases GluA2-mushroom spines and decreases GluA2-filopodia spines in hippocampus CA1. *Hippocampus* **27**, 1224–1229 (2017).
90. J. Wei *et al.*, Estrogen protects against the detrimental effects of repeated stress on glutamatergic transmission and cognition. *Mol. Psychiatry* **19**, 588–598 (2014).
91. E. Choleris, L. A. M. Galea, F. Sohrabji, K. M. Frick, Sex differences in the brain: Implications for behavioral and biomedical research. *Neurosci. Biobehav. Rev.* **85**, 126–145 (2018).
92. S. Kim, E. B. Ziff, Calcineurin mediates synaptic scaling via synaptic trafficking of Ca2+-permeable AMPA receptors. *PLoS Biol.* **12**, e1001900 (2014).
93. K. Sztukowski *et al.*, HIV induces synaptic hyperexcitation via cGMP-dependent protein kinase II activation in the FIV infection model. *PLoS Biol.* **16**, e2005315 (2018).
94. A. Zaytseva, Ketamine's rapid antidepressant effects are mediated by Ca2+-permeable AMPA receptors in the hippocampus. bioRxiv [Preprint] (2023), https://doi.org/10.1101/2022.12.05.519102 (Accessed 16 January 2023).
95. J. Shou, A. Tran, N. Snyder, E. Bleem, S. Kim, Distinct roles of GluA2-lacking AMPA receptor expression in dopamine D1 or D2 receptor neurons in animal behavior. *Neuroscience* **398**, 102–112 (2018).
96. S. Kim *et al.*, Brain region-specific effects of cGMP-dependent kinase II knockout on AMPA receptor trafficking and animal behavior. *Learn. Mem.* **23**, 435–441 (2016).